Quadrupole-quadrupole plus pairing interaction application to transition charge density calculations in some even-even palladium nuclei

A. J. Singh and P. K. Raina
Physics Department, H. P. University, Shimla-171 005, India

S. K. Dhiman
Indira Gandhi National Open University, Shimla-171 004, India

(Received 7 June 1994)

Here we report the microscopic variational model calculations for the recently available experimental data on transition charge densities (TCD) of ^{104,106,108,110}Pd nuclei employing "quadrupole-quadrupole plus pairing interactions" operating in the $2p_{1/2}$, $1g_{9/2}$, $2d_{5/2}$, $3s_{1/2}$, $2d_{3/2}$, $1g_{7/2}$, and $1h_{11/2}$ valance spaces. Results for different p-n interaction strenghts are also given. It is seen that TCD, being sensitive to the strength parameters, can act as one of the best means for the fixing of these parameters accurately. The results of TCD calculations, for quadrupole excitations, using the p-n interaction strength parameter $\chi_{\pi\nu} = -0.0231$ MeV b^{-4}, are in excellent agreement. The calculated static properties from the Hartree-Fock-Bogoliubov (HFB) model, employed for TCD calculations, are also in good agreement. Deivation in the TCD results for hexadecupole transitions points toward the need for some modifications so as to simulate the other interaction effects.

PACS number(s): 21.10.Ft, 21.10.Ky, 21.60.Jz, 25.30.Dh

I. INTRODUCTION

For many years medium mass nuclei have been the center of activities due to the observed variety of phenomena displayed by them. Theoretical attempts are continuously going on for the understanding of these phenomena. The success of the microscopic models is very much dictated by the two-body interactions used in the calculations. Microscopic attempts for the description of spectra, transition probabilities, and moments in the mass region $A = 100$ have proved to be satisfactory through the "quadrupole-quadrupole plus pairing effective interaction."

Electron scattering has some special features [1] that makes it one of the best tools for nuclear structure studies. The electron interacts with the nuclear charge and current distribution through the "well known and weak" electromagnetic interaction. The charge and current distribution, which determine the electron scattering cross sections, are also responsible for gamma-ray transitions, although the higher multipolarity states can rarely be investigated with the help of these transitions. On the other hand, in the case of electron scattering [2,3] the peaks, corresponding to higher l-value transitions, dominate the spectrum at sufficiently high values of momentum transfer q. With the availability of electroexcitation data for $0^+ \rightarrow 4^+$ transitions recently, it has been possible to observe [4] that the rotor model formula does not apply to hexadecupole excitations as such.

Transcription [5–13] of inelastic electron scattering cross section data to the transition charge density, in a model-independent way, for some f-p and s-d-g-h shell nuclei, has made the comparison of theoretical calculations with the experiments more effective. For low-lying collective excitations, where microscopic effects are not dominant, one expects simply a peak in the transition charge density at the surface of the nucleus.

Frequently the sensitive questions regarding the validity of (a) the two-body interaction and (b) the specific microscopic model through which theoreticians calculate the properties of the nuclei, start becoming controversial. Here calculations of the transition charge densities can play an important role since small changes in the system dynamics are very sharply reflected in the magnitude of the surface peak as well as the interior transition charge densities of the nucleus. Such an observation became a reality through the experimental inelastic electron scattering data [13] on germanium nuclei.

By comparing results of model calculations based on different valence spaces with the experimental values, one can investigate the basic properties of the model, like the configuration mixing, which in turn depends on the residual interaction used. Nuclei in the mass region 100 have shown some anomalous features in their properties. One expects that the transition charge density which is the best meeting ground for the theoretical and experimental results on any specific transition, will act as one of the best probes in providing us with a clear picture of the underlying dynamics [7].

Data for transition charge densities have started becoming available for some Ge, Mo, Sr, Zr, Cd, and Pd nuclei [5–10]. The useful shell model calculations are not possible for most of these nuclei and here we have attempted variational model calculations for even-even palladium nuclei. Apart from some calculations of transition charge densities in s-d and f-p shell nuclei with restricted configurations [11–13] and the theoretical prediction with the Hartree-Fock (HF) approximation for the $0^+ \rightarrow 2^+$ transition in ^{154}Gd by Negle and Rinker [14], there have been no reports of microscopic calcula-

tions in other regions. In the medium mass nuclei, the only attempts that have been made are with the interacting boson model (IBM), but this formalism uses a lot of experimental data for parametrizing density functions.

Recently [5,6], data on the transition charge densities for quadrupole and hexadecupole excitation have become available in the case of some palladium nuclei. Here we report the calculations for ^{104,106,108,110}Pd nuclei by the variation after projection method (VAP) in the Hartree-Fock-Bogoliubov (HFB) framework. This is the first time that a microscopic calculation for transition charge densities (TCD's) has been done in this region and the effect of p-n interaction has been studied. It is seen that transition charge density calculations act as a sensitive guide for the role of different parts of the interactions.

II. CALCULATIONAL FRAMEWORK

The single-particle energies (SPE's) that have been employed are (in MeV) $\epsilon(2p_{1/2}) = -0.8$, $\epsilon(1g_{9/2}) = 0.0$, $\epsilon(2d_{5/2}) = 5.4$, $\epsilon(3s_{1/2}) = 6.4$, $\epsilon(2d_{3/2}) = 7.9$, $\epsilon(1g_{7/2}) = 8.4$, and $\epsilon(1h_{11/2}) = 8.8$. The same set of SPE's has been employed in a number of successful shell model as well as variational model calculations for static properties in the mass 100 region by Vergados and Kuo [15] and Federman and Pittel [16] as well as Khosa, Tripathi, and Sharma [17].

The pairing part of the two-body interaction can be written as

$$V_P = -(G/4)\sum_{\alpha\beta} S_\beta S_\alpha a^\dagger_\alpha a^\dagger_{\bar\alpha} a_\beta a_{\bar\beta},$$

where α denotes the quantum numbers $(nljm)$. The state $\bar\alpha$ is the same as α but with the sign of m reversed. Here S is the phase factor $(-1)^{j-k}$. The q-q part of the two-body interaction is given by

$$V_{q-q} = -(\chi/2)\sum_{\alpha\beta\gamma\delta}\sum_{\mu}\langle\alpha|q^2_\mu|\nu\rangle\langle\beta|q^2_{-\mu}|\delta\rangle \times(-1)^\mu a^\dagger_\alpha a^\dagger_\beta a_\delta a_\gamma,$$

where the operator q^2_μ is given by $q^2_\mu = (16\pi/5)^{1/2} r^2 Y^2_\mu(\theta,\phi)$.

The strengths for the like particles n-n and p-p components of the q-q interaction are taken as $\chi_{\pi\pi}(=\chi_{\nu\nu}) = -0.0105$ MeV b^{-4} and the effect of the n-p components of the interaction has been checked for three values of $\chi_{\pi\nu} = -0.0231$, -0.0250, and -0.0300 MeV b^{-4}. Here b is the oscillator parameter. These values for the strengths of the q-q interactions are comparable to those suggested by Arima [18] on the basis of an empirical analysis of the effective interactions. The strength of the pairing interaction was fixed (through the approximate relation $G = 18/A$) at $G = 0.18$ MeV.

The axially symmetric intrinsic deformed HFB state with $K = 0$ can be written

$$|\phi_0\rangle = \prod_{im}(U^m_i + V^m_i b^\dagger_{im} b^\dagger_{i\bar m})|0\rangle, \quad (1)$$

where

$$b^\dagger_{im} = \sum_j C^m_{ji} a^\dagger_{jm},$$

$$b^\dagger_{i\bar m} = \sum_j (-1)^{j-m} C^m_{ji} a^\dagger_{j-m}. \quad (2)$$

Here, the index i is used to distinguish between different states with the same m, and j labels the spherical single particle orbitals. The wave function in Eq. (1) can be reduced to the form

$$|\phi_0\rangle = N\exp\left[\tfrac{1}{2}\sum_{\alpha\beta} f_{\alpha\beta} a^\dagger_\alpha a^\dagger_\beta\right]|0\rangle \quad (3)$$

with

$$f_{\alpha\beta} = \sum_i C^{m_\alpha}_{j_\alpha i} C^{m_\beta}_{j_\beta i}(V^{m_\alpha}_i/U^{m_\alpha}_i)\delta_{m_{\alpha'}-m_\beta}, \quad (4)$$

where α denotes the quantum numbers $(j_\alpha m_\alpha)$ and N is the normalization constant.

The state with angular momentum J is given by

$$|\psi^J_{K=0}\rangle = N\int d\Omega\, d^J_{00}\exp\left(\sum_{\alpha\beta} F_{\alpha\beta}(\theta)\right) a^\dagger_\alpha a^\dagger_\beta|0\rangle, \quad (5)$$

where

$$F_{\alpha\beta} = \sum_{m'_\alpha}\sum_{m'_\beta} d^{J_\alpha}_{m_\alpha m'_\alpha}(\theta) d^{J_\beta}_{m_\beta m'_\beta}(\theta) f_{j_\alpha m'_\alpha, j_\beta m'_\beta}. \quad (6)$$

The expression for the overlap $\langle\psi^J_0|\psi^J_0\rangle$ is given by (apart from the normalization N)

$$n(\theta) = \langle\psi^J_0|\psi^J_0\rangle = [\det(1 + M(\theta))]^{1/2}, \quad (7)$$

where

$$M(\theta) = F(\theta) f^\dagger. \quad (8)$$

The energy of a state with angular momenta J can be written as

$$E_J = \left[\int_0^\pi d\theta \sin\theta d^J_{00}(\theta) h(\theta)\right] \Big/ \left[\int_0^\pi d\theta \sin\theta d^J_{00}(\theta) n(\theta)\right]. \quad (9)$$

The intensities of the various angular momenta contained in the intrinsic wave function are given by

$$a^2_J = \tfrac{1}{2}(2J+1)\int_0^\pi n(\theta) d^J_{00}(\theta)\sin\theta\, d\theta. \quad (10)$$

The overlap integral $h(\theta)$ is given by

$$h(\theta) = n(\theta)\Bigg(\sum_{\alpha} e_\alpha [M/(1+M)]_{\alpha\alpha} + \tfrac{1}{4}\sum_{\alpha\beta\gamma\delta}\langle\alpha\beta|V_A|\gamma\delta\rangle \times\{2[M/(1+M)]_{\gamma\delta}[M/(1+M)]_{\delta\beta} + \sum_{\nu\rho}[M/(1+M)]_{\gamma\rho}F_{\rho\delta}[1/(1+M)]_{\nu\alpha}f^*_{\nu\beta}\}\Bigg) \quad (11)$$

and the overlap integrals $n(\theta)$ and $M(\theta)$ are given by Eqs. (7) and (8).

The VAP procedure involves the selection of an appropriate intrinsic state for each yrast level through a minimization of the expectation value of the Hamiltonian with respect to the states of good angular momentum. We first generate self-consistent HFB solutions $\phi(\beta)$, by carrying out HFB calculations with the Hamiltonian $(H - \beta Q_0^2)$. The optimum intrinsic state for each yrast level, $\phi_{\rm opt}(\beta_J)$, is then selected by ensuring that the following condition is satisifed:

$$[\langle\phi(\beta)|HP^J_{00}|\phi(\beta)\rangle/\langle\phi(\beta)|P^J_{00}|\phi(\beta)\rangle] = 0.$$

The transition charge density $\rho_L(r)$, the reduced matrix elements of $\rho_L^{\rm opt}$, is given by

$$\rho_L(r) = \langle J_f||\rho_L^{\rm opt}||J_i\rangle. \quad (12)$$

Making use of the general expression [19] for the matrix elements of an irreducible tensor and Eq. (5) for the projected HFB wave functions, we obtained the following expression for transition charge density:

$$\rho_L(J_i \to J_f) = (n^{J_f}n^{J_i})^{-1/2}(2J_i+1)^{-1/2}\int_0^{\pi/2}\sum_{\mu}\begin{vmatrix} J_i & L & J_f \\ -\mu & \mu & 0\end{vmatrix} d^J_{-\mu,0}(\theta)n(\theta)\Bigg\{\sum_{k\alpha\beta} e_k R_{n_\alpha 1_\alpha}(r) \times R_{n_\beta 1_\beta}(r)\langle\alpha|Y^L_M|\beta\rangle M(\theta)[1+M(\theta)]^{-1}\Bigg\}\sin(\theta)\,d\theta, \quad (13)$$

where $R_{nl}(r)$ is the radial part of the harmonic oscillator state $|nl\rangle$ and the normalizations are given by

$$n^J = \int_0^{\pi/2} n(\theta)d^J_{00}(\theta)\sin\theta\,d\theta, \quad (14)$$

$$n(\theta) = \{\det[1+M(\theta)]\}^{1/2}. \quad (15)$$

The expression for the reduced transition probability for the electric 2^L-pole, $B(EL, 0^+ \to 2^+)$ and the static quadrupole moments for the L^+ state, Q_{L^+}, are given by

$$B(EL, 0^+ \to L^+) = (1/16\pi)|\langle\psi^L_0||Q^L_0||\psi^0_0\rangle|^2, \quad (16)$$

$$Q_{L^+} = \langle\psi^L_L|Q^L_0|\psi^L_L\rangle,$$

where

$$Q^L_\mu = (16\pi/2L+1)^{1/2}r^L Y^L_\mu(\Omega). \quad (17)$$

The expression for reduced matrix elements of transition probability

$$\langle J_f|Q^L_0|J_i\rangle = [n^{J_f}n^{J_i}]^{-1/2}\int_0^{\pi/2}\sum_{\mu}\begin{vmatrix} J_i & L & J_f \\ -\mu & \mu & 0\end{vmatrix} \times d^J_{-\mu 0}(\theta)n(\theta)\Bigg\{\sum_{k\alpha\beta} e_k\langle n_\alpha 1_\alpha|r^L|n_\beta 1_\beta\rangle \times\langle\alpha|Y^L_M|\beta\rangle\rho^k_{\alpha\beta}(\theta)\Bigg\}\sin\theta\,d\theta, \quad (18)$$

where the density matrix is given by

$$\rho(\theta) = M(\theta)/[1+M(\theta)]. \quad (19)$$

The initial guess for the wave functions involved in HFB iterations was generated by diagonalizing the Nilsson Hamiltonian and the wave functions $|\phi\rangle$ are obtained by carrying out the HFB calculations. The results of HFB calculations are summarized in terms of the expansion coefficients C^m_{ji} and the amplitudes (V^m_i, U^m_i) appearing in Eq. (1).

These values were used first to calculate f defined by Eq. (4). We next calculate the matrices F, $[1+M(\theta)]$ and $[1+M(\theta)]^{-1}$, appearing in the Eqs. (6), (7), and (8), respectively. Finally we compute the matrix element for transition charge densities and transition probabilities in Eqs. (13) and (18).

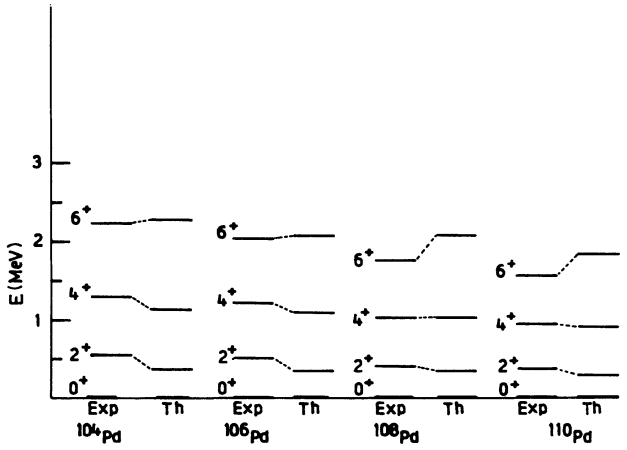

FIG. 1. Experimental spectra of low-lying states of ^{104,106,108,110}Pd isotopes along with theoretical results in the VAP on HFB states.

TABLE I. The intrinsic quadrupole moments of the HFB states in some doubly even-even PD isotopes. Here $\langle Q_0^2\rangle_\pi$ ($\langle Q_0^2\rangle_\nu$) gives the contribution of the protons (neutrons) to the total intrinsic quadrupole moment. The quadrupole moments have been computed in units of b^2.

Set No.	Nucleus	$E_{\rm HFB}$	$\langle Q_0^2\rangle_{\rm HFB}$	$\langle Q_0^2\rangle_\pi$	$\langle Q_0^2\rangle_\nu$
1	^{104}Pd	31.92	57.12	22.11	35.01
2	^{106}Pd	44.04	58.59	21.99	36.59
3	^{108}Pd	58.31	61.76	22.52	39.24
4	^{110}Pd	72.62	63.32	22.79	40.53

III. RESULTS AND DISCUSSION

Here, in this section we compare the experimental results on static properties, like energy spectra, transition probabilities, and static moments, and the recently [3,4] available data on the transition charge densities for quadrupole and hexadecupole excitation for ^{104,106,108,110}Pd nuclei, with our theoretical results by the VAP in the HFB framework. This is the first time that any microscopic calculation has been attempted for studying TCD's of these nuclei. In the shell model calculations, the number of configurations that can be taken into account must be limited for computational reasons. The only attempt made for the description of TCD is with the IBM formalism where large experimental data sets have been used for parametrizing the density functions.

A. Yrast spectrum, static quadrupole moments, and transition probabilities

The results of calculations of the yrast spectrum for ^{104,106,108,110}Pd nuclei are shown in Fig. 1, and it is seen that they are in good agreement with the experimental results.

In Table I we have given the calculated HFB values for total energy ($E_{\rm HFB}$) and quadrupole moment ($\langle Q_0^2\rangle_{\rm HFB}$) along with the separate contribution of protons as well as neutrons. Here we see that the quadrupole moment shows a regular increase in going from ^{104}Pd to ^{110}Pd. These changes can be understood in terms of the occupation numbers of protons and neutrons in the different shells. We notice from the Tables II(a) and II(b) that in going from ^{104}Pd to ^{110}Pd, there is not much transition of protons into different orbits and additional neutrons keep distributing into the $d_{5/2}$, $g_{7/2}$, and $h_{11/2}$ orbits. Figure 2 makes these observations very clear.

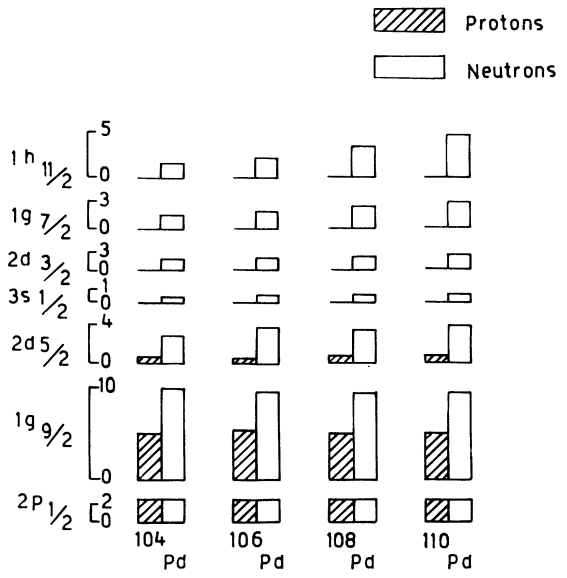

FIG. 2. Theoretical results of subshell occupation numbers in the ground states of Pd isotopes.

Next, we have a look at the results for reduced transition probabilities $B(E2)$ which are given in Table III. Here, we see that the effective charges, which incorporate the core polarization in a simple way, provide quite satisfactory matching with experimental results for very reasonable values; 0.4 for ^{104}Pd and 0.5 for other Pd isotopes. The results for static quadrupole moments for 2^+ states are presented in Table IV. Here, one notices the similar behavior as seen in the case of the $B(E2; 0^+ \rightarrow 2^+)$ values for these nuclei.

TABLE II. The calculated values of the occupation numbers of various orbits in the ground states of some Pd isotopes for (a) protons and (b) neutrons.

Set No.	Nucleus	$3s_{1/2}$	$2p_{1/2}$	$2d_{3/2}$	$2d_{5/2}$	$1g_{7/2}$	$1g_{9/2}$	$1h_{11/2}$
				(a)				
1	^{104}Pd	0.06	2.00	0.03	0.71	0.04	5.14	0.00
2	^{106}Pd	0.06	2.00	0.03	0.70	0.04	5.17	0.00
3	^{108}Pd	0.07	1.99	0.03	0.75	0.05	5.08	0.00
4	^{110}Pd	0.08	1.99	0.04	0.79	0.05	5.04	0.00
				(b)				
1	^{104}Pd	0.69	1.99	1.34	2.29	1.51	9.83	1.64
2	^{106}Pd	0.75	1.99	1.40	3.36	1.95	9.84	2.69
3	^{108}Pd	0.84	1.99	1.48	3.64	2.50	9.85	3.68
4	^{110}Pd	0.96	1.99	1.56	4.02	3.00	9.87	4.58

TABLE III. Comparison of the calculated and observed $B(E2, 0^+ \rightarrow 2^+)$ values in some Pd isotopes. The effective charges have been used such that for protons the effective charge is $e_\pi = 1 + e_{\text{eff}}$ and for neutrons it is $e_\nu = e_{\text{eff}}$. The values of the oscillator parameter have been calculated from the relation $b = 1.01A^{1/6}$ fm.

Set No.	Nucleus	$B(E2, 0^+ \rightarrow 2^+) \times 10^{-50} e^2(\text{cm}^4)$ Calculated e_{eff} 0.4	0.5	0.6	Expt.
1	^{104}Pd	49.97	63.40	78.41	51.0 ± 5.0[a]
					53.0 ± 3.0[b]
2	^{106}Pd	51.80	65.93	90.00	61.0 ± 6.0[a]
					62.0 ± 4.0[b]
3	^{108}Pd	56.33	71.94	89.44	70.0 ± 7.0[a]
					73.0 ± 5.0[b]
4	^{110}Pd	59.08	75.58	94.11	82.0 ± 8.0[a]
					86.0 ± 6.0[b]

[a]G. Ripka, Adv. Nucl. Phys. **1**, 183 (1968).
[b]Alan Christy and O. Hausser, Nucl. Data Tables **11**, 281 (1972).

TABLE IV. Comparison of the calculated and observed $Q(2_1^+)$ values in some Pd isotopes. The effective charges have been used such that for protons the effective charge is $e_\pi = 1 + e_{\text{eff}}$ and for neutrons it is $e_\nu = e_{\text{eff}}$.

Set No.	Nucleus	$Q(2_1^+) \times e$ (fm^2) Calculated e_{eff} 0.1	0.2	0.3	0.4	Expt.
1	^{104}Pd	−0.39	−0.48	−0.56	−0.63	-0.25 ± 0.12[a]
						-0.47 ± 0.10[b]
						-0.25 ± 0.12[c]
						-0.21 ± 0.07[d]
2	^{106}Pd	−0.40	−0.49	−0.57	−0.55	-0.49 ± 0.06[a]
						-0.52 ± 0.12[c]
						-0.56 ± 0.08[d]
3	^{108}Pd	−0.41	−0.50	−0.59	−0.67	-0.54 ± 0.06[a]
						-0.51 ± 0.06[d]
						-0.60 ± 0.12[e]
4	^{110}Pd	−0.42	−0.51	−0.60	−0.69	-0.60 ± 0.12[a]
						-0.55 ± 0.08[d]
						-0.72 ± 0.14[e]

[a]Alan Christy and O. Hausser, Nucl. Data Tables **11**, 281 (1972).
[b]S. Landsberger, R. Lecomte, P. Paradis, and S. Monaro, Phys. Rev. C **21**, 588 (1980).
[c]A. M. Kleinfeld, private communication to L. Hasselgren, Uppsala University, Institute of Physics Report No. UUIP 987, 1979 (unpublished).
[d]M. F. Nolen, J. Hall, D. J. Thomas, and M. J. Throop, J. Phys. A **6**, 57 (1973).
[e]A. Bockisch, private communication to L. Hasselgren, Uppsala University, Institute of Physics Report No. UUIP 987, 1979 (unpublished).

B. Transition charge densities

Our transition charge density results for the $0^+ \rightarrow 2_1^+$ transitions of Pd isotopes, as seen from Figs. 3 and 4, have a characteristic surface peak at 5 fm and some small fluctuations in the interior. The only available experimental results for quadrupole excitation of ^{106,110}Pd are also plotted. One observes that the results for ^{110}Pd are in excellent agreement with the recent experimental ones for $\chi_{\pi\nu} = -0.0231$ MeV b^{-4}. The experimental results [20] in case of ^{106}Pd have been extracted from the energy transfer data between 0.6 and 1.8 fm^{-1} only. Here, one can only compare the surface peak of TCD's and we again notice excellent agreement with the same value of $\chi_{\pi\nu}$. The experimental results of other Pd isotopes are not reported in the literature; we expect these results also to agree well with experiments. The energy spectra also show such features, but in the case of the transition charge density, the results are more prominent.

The hexadecupole states projected from the same HFB wave function, used for quadrupole excitations were also used to calculate the transition charge densities for $0^+ \rightarrow 4_1^+$ excitations. The experimental as well as theoretical

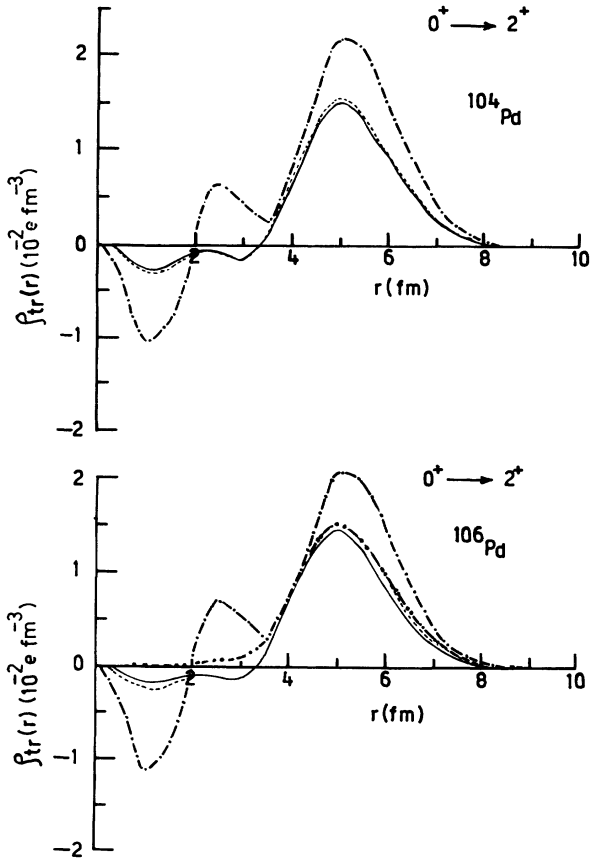

FIG. 3. Transition charge densities for $0^+ \rightarrow 2_1^+$ excitations of ^{104,106}Pd isotopes in the HFB framework. Solid, dashed, and dashed lines with single dot represent the curves for $\chi_{\pi\nu} = -0.0231, -0.0250$, and -0.0300 MeV b^{-4}, respectively. Curve with dash and double dots represents the experimental result for ^{106}Pd.

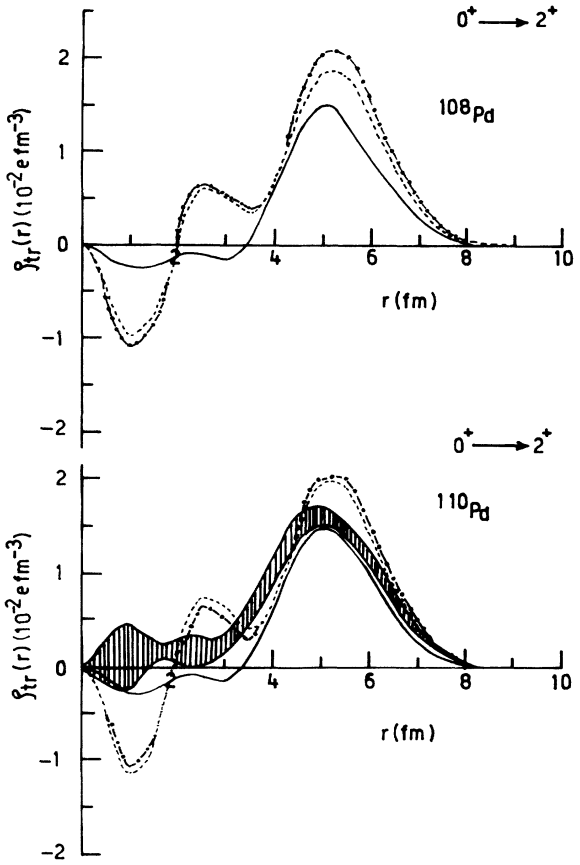

FIG. 4. Transition charge densities for $0^+ \rightarrow 2_1^+$ excitations of ^{108,110}Pd isotopes in the HFB framework. Solid, dashed, and dashed lines with single dot represent the curves for $\chi_{\pi\nu} = -0.0231, -0.0250$, and -0.0300 MeV b^{-4}, respectively. Curve with error bars represents the experimental result for ^{110}Pd.

results for $0^+ \rightarrow 4_1^+$ transition charge densities of ^{104}Pd isotope are shown in Fig. 5. We notice some interesting features in the interior of this nucleus. Theoretical results too exhibit these features qualitatively, characterized through one negative peak around 4 fm and one positive peak around 6 fm. However, theoretical results show shifting of the peaks by approximately 1 fm to the left. The effect of changes of $\chi_{\pi\pi}$, $\chi_{\nu\nu}$, and pairing strength was also tried. It is observed that there is change only in magnitude of the peak, but the shift in the peak is not affected at all. Here we have not shown the results for hexadecupole excitations for other isotopes, since the results also show similar deviations in all the cases. The yrast spectra for these states are in good agreement with the experimental values and hence it does tell us that the dynamic properties, in contrast to the static properties, do need deeper studies of the model and the interactions. Some of the possibilities are the inclusion of the higher multiplole interactions, like hexadecupole-hexadecupole interactions, and renormalizations of the cores which do not show any effects on the quadrupole properties of these

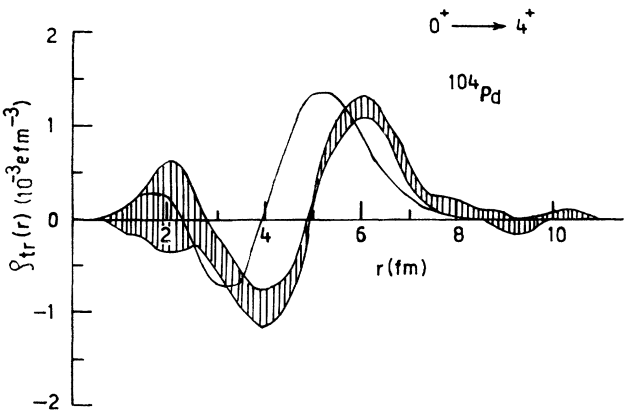

FIG. 5. Transition charge densities for $0^+ \rightarrow 4_1^+$ excitation in the case of the ^{104}Pd nucleus. Solid line represents the curve for $\chi_{\pi\nu} = -0.0231$ MeV b^{-4}. Curve with error bars represents the experimental results.

nuclei. Some of these ideas are under study and will be reported in future.

IV. CONCLUSIONS

The results discussed above clearly show that the "quadrupole-quadrupole plus pairing interactions," which have been used extensively for the calculation of static properties, are also successful for the calculation of transition charge density for the quadrupole excitations to a great extent, but show some discrepancies for hexadecupole excitation in the case of palladium isotopes. From these results it can be concluded that the realistic interaction is expected to be mainly of this type, whereas some part of it is missing which has given rise to the discrepancies for the hexadecupole excitations. It has been pointed out in some of the earlier observations [21,22] of medium mass nuclei that the contribution of higher multipole interactions with different neutron-proton interaction strength plays some important role. This can be true for the nuclei under our consideration too. The contribution of the secondary effects of subnucleonic particles to the realistic interactions may also be affecting the transition charge density results.

ACKNOWLEDGMENTS

One of the authors (P.K.R.) would like to thank DST for grants for the research project. S. K. Dhiman is also thankful to U.G.C. for the financial assistance. The authors are grateful to Professor S. P. Pandya and Professor S. K. Sharma for stimulating discussions at IIT Kanpur, and to Professor M. B. Banarjee for going through the manuscript.

[1] H. Uberall, *Electron Scattering From Complex Nuclei* (Academic, New York, 1971), Parts A and B.
[2] J. Heisenberg and H. P. Block, Annu. Rev. Nucl. Part. Sci. **33**, 569 (1983).
[3] J. Heisenberg, Adv. Nucl. Phys. **12**, 61 (1981).
[4] S. K. Sharma and P. K. Raina, Phys. Rev. C **42**, 635 (1990).
[5] J. Wesseling, C. W. De Jager, H. De Vries, M. N. Harakeh, R. De Leo, and M. Pignanelli, Phys. Lett. B **245**, 338 (1990).
[6] J. Wesseling *et al.*, Nucl. Phys. **A535**, 285 (1991).
[7] B. Frois and C. N. Papanicolas, Annu. Rev. Nucl. Part. Sci. **37**, 133 (1987).
[8] J. P. Bazantay, J. M. Cavedon, J. C. Clemens, B. Frois, D. Goutte, M. Huet, P. Leconte, Y. Mizuno, X. H. Phan, and S. K. Platchkov, Phys. Rev. Lett. **54**, 643 (1985).
[9] T. E. Milliman, J. P. Connelly, J. H. Heisenberg, F. W. Hersman, J. E. Wise, and C. N. Papanicolas, Phys. Rev. C **41**, 2586 (1990).
[10] J. P. Connelly, T. E. Milliman, J. H. Heisenberg, F. W. Hersman, J. E. Wise, and C. N. Papanicolas, Phys. Rev. C **42**, 1948 (1990).
[11] R. Neuhausen, Nucl. Phys. **A282**, 225 (1977).
[12] R. B. M. Mooy and P. W. M. Glaudemans, Nucl. Phys. **A438**, 461 (1985).
[13] P. K. Raina and S. K. Sharma, Phys. Rev. C **37**, 1427 (1988).
[14] J. W. Negele and G. Rinker, Phys. Rev. C **15**, 1499 (1977).
[15] J. D. Vergados and T. T. S. Kuo, Phys. Lett. **35B**, 93 (1971).
[16] P. Federman and S. Pittel, Phys. Lett. **77B**, 29 (1978).
[17] S. K. Khosa, P. N. Tripathi, and S. K. Sharma, Phys. Lett. **119B**, 257 (1982).
[18] A. Arima, Nucl. Phys. **A354**, 19 (1981).
[19] N. Onishi and S. Yoshida, Nucl. Phys. **A80**, 367 (1966).
[20] K. Hosoyama, Y. Torizuka, Y. Kawazoe, and H. Ui, Phys. Rev. Lett. **30**, 388 (1973).
[21] J. A. Sheikh *et al.*, Phys. Rev. Lett. **64**, 376 (1990).
[22] A. Etchegoyen, P. Federman, and E. G. Vergini, Phys. Rev. C **39**, 1130 (1989).